Molecular Dynamics Study of Hexadecane Droplets: Kinetics and Mechanism of Freezing

Sonya Tsibranska-Gyoreva,*[,a] Stoyan Iliev,[b] Slavka Tcholakova,[a] Anela Ivanova,[b] Nikolai Denkov[a]

[a]*Department of Chemical and Pharmaceutical Engineering, and* [b]*Department of Physical Chemistry, Faculty of Chemistry and Pharmacy, Sofia University "St. Kliment Ohridski", 1 James Bourchier blvd., 1164 Sofia, Bulgaria*

**Corresponding author: st@lcpe.uni-sofia.bg*

Abstract

This work presents results, aimed at identifying the crystallization mechanism of surfactant-stabilized hexadecane-in-water droplet with 15 nm diameter at the molecular-level. The question is addressed by atomistic molecular dynamics simulations of models consisting of ca. 2 million atoms. To represent as closely as possible real-world systems, a procedure for constructing droplets of different sizes is developed, allowing control of the surfactant surface coverage. Two crystallization protocols are applied: slow freezing, in which the surface solidifies first, followed by relaxation and subsequent cooling to induce crystallization in the bulk, and fast freezing, in which the droplet is directly cooled to the final temperature, leading to simultaneous surface and core crystallization.

A few key results may be outlined. The droplet surface always freezes first. Nucleation occurs stochastically at multiple independent sites, gradually propagating over the surface. Both shell and core undergo heterogeneous nucleation initiated by surfactant molecules. The nuclei in the core typically form close to the surface. The cooling procedure affects the spatial freezing pathway and molecular ordering in the drop core. The preferred orientation of bulk crystallites relative to the originating surface is nearly perpendicular. Once solidified, the surface alone is sufficient to induce droplet deformation to a triangular prism-like shape, additionally stabilized by the bulk crystallites. The deformation is a clear indication of a rotator phase, stable over hundreds of nanoseconds, further confirmed by the fraction of *gauche* conformations, P_2 order parameters, and radial distribution functions. These findings agree with and complement experimental data and provide molecular-level verification of the experimentally observed fundamental difference in the stability of hexadecane rotator phase: transient in bulk and stable under micro- and nano-confinement. They enhance the fundamental knowledge on microscopic freezing mechanisms of hexadecane and similar even-parity alkane-based materials at interfaces.

Keywords

Drop, hexadecane, rotator phase, molecular dynamics, structural analysis

Introduction

Molecular dynamics (MD) simulations of droplets are widely used to investigate various processes where detailed molecular-level information is required and cannot be easily obtained from experiments. In the literature, droplet simulations are most commonly associated with studies of their behavior in electric fields, emulsification processes, droplet break-up, collision and coalescence, spreading and wetting phenomena, as well as the freezing of water droplets [1-19].

Simulations of phase transitions in droplets using molecular dynamics are relatively scarce [14, 20, 21]. In particular, phase transitions of alkanes in droplets have not been investigated with atomistic MD so far. Experimental studies, however, show that droplets, similarly to other micro and nano confinements, such as porous materials, can strongly influence the phase transition temperatures, phase formation and stability [22-38]. For example, Huber et al. observed significant supercooling of alkanes confined in SiO_2 pores, with the temperature shift approximately proportional to the inverse mean pore diameter [25]. Confinement was also found to stabilize intermediate rotator phases that are unstable or only transient in bulk systems [25-27]. Similar effects have been observed in experiments with alkanes confined in polymeric microcapsules [30, 31] and emulsion droplets [36-38], where confinement and type of surfactant used to stabilize the emulsion promote the formation of rotator phases and significantly modify the crystallization mechanism compared to bulk systems [36, 37]. These studies demonstrate that both the geometry of confinement and the chemical nature of the confining interface strongly affect the phase behavior of alkanes.

In our previous studies [39-42], we performed atomistic molecular dynamics simulations to investigate the phase transitions of pure bulk pentadecane and hexadecane (HEX), as well as systems pentadecane/surfactant($C_{16}EO_2$)/water and hexadecane/surfactant($C_{16}EO_2$)/water with flat interfaces. Starting from the isotropic liquid phase, we simulated the cooling process and analyzed the mechanism of crystallization and the structuring of the resulting solid-state configurations. Our results demonstrated that the developed computational protocol reliably captures the crystallization process in all studied systems, including the formation, type and stability of rotator phases, and allows assessment of the effect of chain parity on the crystallization behavior.

The next logical step is to examine the behavior of the molecules when the model system is a droplet stabilized with the same surfactant. In particular, we aim to investigate the mechanism of crystallization in hexadecane droplets and to determine whether changes in droplet shape occur during the phase transition, similar to those observed in experiments [43].

One of the important parameters, allowing meaningful comparison between MD simulation results and experimental data, is the spherical shape of the droplet. To obtain a spherical geometry, different authors employ a variety of techniques and methodologies [1-13]. One frequently used

approach for generating spherical model structures is to build the droplet with the package Packmol [1-4]. Packmol is commonly used to generate initial configurations for MD simulations by packing molecules into predefined spatial regions. It ensures a random distribution of molecules while maintaining a user-defined minimum intermolecular distance (tolerance), thus preventing strong short-range repulsive interactions that could destabilize the simulation.

Another widely used approach is first to construct a system that approximates the desired droplet composition and simulate it until stable bulk properties are achieved. The resulting system can then be placed in a larger simulation box and hydrated, leading to the formation of a droplet that gradually adopts a spherical shape [5-9]. In some studies, the droplet is initially placed on a surface in a cubic configuration and, even in the absence of surrounding water, it can evolve into spherical shape during the relaxation and spreading process [10].

Other procedures for droplet construction are also reported in the literature. One approach involves arranging molecules in an initial face-centered cubic (FCC) configuration, which is subsequently MD-equilibrated to obtain a liquid droplet [11]. In other simulations, oil molecules and water are initially placed together in the simulation box, leading to the aggregation of the oil molecules and to spontaneous formation of a droplet [12]. In some cases, molecules located outside a predefined spatial region are removed to obtain a structure with the desired geometry [13]. However, since these procedures are often not described in sufficient detail in the published studies, reproducing or fully understanding the exact droplet-building protocol can be challenging. The construction of surfactant-stabilized droplets is also an important aspect for MD simulations. In the literature, three main approaches are typically employed: (1) the surfactant molecules are placed directly on the droplet surface in the initial configuration [2, 4] (2) individual surfactant monomers are added to the system and allowed to adsorb onto the droplet surface, or they are initially positioned as a layer and subsequently migrate and adsorb onto the surface [3, 6, 8, 12], and (3) a micelle is constructed that subsequently coalesces with the droplet [5, 7].

In the latter two approaches, adsorption is needed, which is a relatively slow process. When surfactant monomers are used, the formation of a dense interfacial layer can be particularly slow and difficult to achieve within reasonable simulation times. In addition, this method does not allow straightforward control over the degree of surfactant surface coverage of the droplet.

In the present work, we develop a new procedure for constructing emulsion droplets that allows precise control over the number of surfactant molecules placed at the droplet surface and remains applicable even at very high surface concentrations. A droplet with a diameter d = 15 nm is constructed and studied under two different temperature regimes: slow freezing (performed in two steps, from 350 to 300 K, followed by equilibration at 300 K, and then from 300 to 278 K) and fast freezing (from 350 directly to 278 K). In addition, we devise analysis procedures (described in

the Supporting Information, Section: Analysis procedures) for identifying crystallization processes in alkane droplets, which are also applicable to droplets composed of other molecules.

The simulations advance the current knowledge by revealing the mechanism of crystallization both on the hexadecane droplet surface and in the droplet interior, as well as the associated droplet deformation during freezing. The influence of spherical confinement is assessed. The obtained molecular-level description provides an explanation of several experimentally observed features [43], including the formation of rotator phases, droplet deformation, and the mechanism of freezing.

Materials and Methods

The results presented in this study are based on a droplet model system. The system consists of 2791 hexadecane molecules and 3000 $C_{16}(EO)_2$ surfactant molecules, hydrated with 409 657 water molecules (Figure 1), resulting in a system containing approximately 2×10^6 atoms.

The number of surfactant molecules was estimated from the droplet surface area. According to the experimental data available in the literature [44, 45], the area occupied by a $C_{16}EO_2$ molecule at the oil/water interface is approximately 0.20 nm², and this value is adopted in the present work. The simulated droplet contained 2791 hexadecane molecules and had a diameter of 15 nm, corresponding to a surface area of approximately 707 nm². Assuming complete interfacial coverage, this surface area corresponds to 3534 surfactant molecules.

However, the adsorption layer at alkane/water interfaces is known to contain both surfactant and alkane molecules, with the reported alkane-to-surfactant ratio ranging from 1:2 to 1:4 [45]. Based on the highest surfactant coverage of 1:4, approximately 80% of the available interfacial sites are expected to be occupied by surfactant molecules, corresponding to 2827 $C_{16}EO_2$ molecules. To ensure complete surface coverage of the droplet in the initial configuration, an additional 5% excess of surfactant was included, resulting in a total of 3000 $C_{16}EO_2$ molecules.

An important advantage of this protocol is that it relies solely on the droplet size and is therefore readily transferable to droplets of different diameters and chemical compositions. Consequently, droplets of different sizes can be constructed using the same methodology while maintaining similar interfacial coverage, thereby enabling direct comparison of their crystallization behavior.

The droplet is constructed using a multistep procedure. Initially, a cubic simulation box with dimensions 30 × 30 × 30 nm, corresponding to twice the desired droplet diameter, is generated, so that a sphere of the target size could be inscribed within the box even after relaxation. The maximum number of hexadecane molecules that could fit without overlaps or unfavorable contacts are randomly placed in the box. The enlarged initial box ensures that after equilibration and box contraction the system will still be larger than the droplet diameter.

The resulting system is energy-minimized, heated to 350 K, and equilibrated for min. 50 ns in NPT ensemble at 1 bar. The equilibration is continued until the system reaches the density of bulk hexadecane. If there is no reference density for the particular system, the equilibration is extended until stable volumetric parameters of the box are obtained.

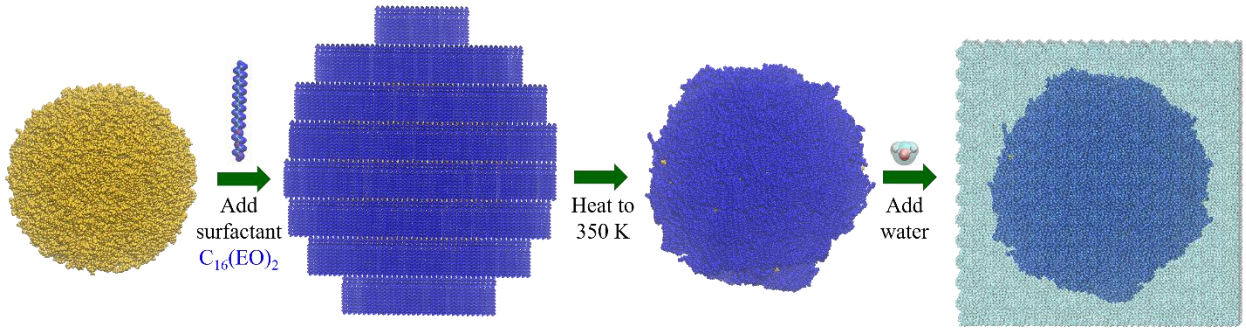

Figure 1. Illustration of the procedure to generate the initial configuration of the studied model droplet; color coding: hexadecane – yellow; $C_{16}(EO)_2$ surfactant – blue; water – cyan.

After equilibration, a spherical region with a diameter of 15 nm is extracted from the equilibrated system using VMD, yielding a hexadecane droplet of the desired size (Figure 1, leftmost picture). Care is taken that molecules are not broken. When droplets of different sizes are required, only the largest system may be simulated using the procedure described above, and droplets of smaller sizes can be extracted subsequently from this equilibrated configuration.

The obtained spherical droplet is then centered in a larger simulation box. The box size is chosen based on the size of the surfactant molecules. In the present study, the surfactant is $C_{16}(EO)_2$, with molecular length of approximately 3 nm. In addition, at least 2 nm of water is required between the droplet and the periodic boundaries to avoid interactions with periodic images. Consequently, a cubic box of 25 × 25 × 25 nm (15 nm droplet diameter plus ~5 nm from each side) is used.

The surfactant molecules are added in the second step, using the *gmx solvate* command to construct a shell containing the desired number of surfactant molecules around the droplet (2^{nd} step in Figure 1). The obtained system is then energy-minimized and heated to 350 K to melt the surfactant layer and smoothen the droplet surface (3^{rd} step in Figure 1). For other surfactants, the temperature should be chosen so that the surfactant phase remains fluid.

The system is then hydrated with explicit water molecules. During this step, some water molecules are placed into the droplet interior. In our protocol, these water molecules are removed using a script in VMD by preserving only water molecules located more than 5 Å away from hexadecane and surfactant molecules, thus retaining the water outside the drop only and removing entirely the artificially included water inside the hexadecane drop. This correction is performed

only once during the preparation of the initial configuration to obtain a physically realistic starting system. The droplet, surfactant, and the hydrating water molecules form the final model system (4^{th} step in Figure 1).

After construction, the system is energy-minimized and heated to 350 K (where both HEX and $C_{16}(EO)_2$ are in liquid state) at a rate of 1 $K.ps^{-1}$ in the NVT ensemble, followed by a 600 ns equilibration at 350 K in the NPT ensemble at 1 bar. The equilibration is verified by tracking the evolution of total energy, temperature, pressure, density, and RMSD of droplet atomic coordinates.

Two different freezing protocols are then applied:

1. *Slow freezing*: the system is first cooled from 350 K to 300 K at a cooling rate of 1 $K.ps^{-1}$ and equilibrated at 300 K for 600 ns. It is then cooled to 278 K using the same cooling rate and simulated for additional 500 ns.
2. *Fast freezing*: the system is cooled directly from 350 K to 278 K using a cooling rate of 1 $K.ps^{-1}$, followed by a 500 ns production simulation.

The final temperature of 278 K is selected based on our previous study [40].

The two protocols were designed to examine the effect of cooling type on crystallization. In the slow freezing, the droplet surface is expected to freeze first, followed by the droplet interior, whereas in the fast protocol freezing occurs throughout the entire droplet concurrently. The two cooling protocols are designed to reproduce the characteristic crystallization processes associated with slow and fast experimental cooling, rather than to match the absolute experimental cooling rates, which are beyond the timescales accessible by atomistic molecular dynamics simulations. In the slow-cooling protocol, the system was first partially cooled from 350 K to 300 K to freeze only the droplet surface – a situation consistent with experimental observations, in which the surface freezing precedes bulk crystallization [43]. Relaxing the system at 300 K then allowed the crystallization to propagate gradually into the droplet interior. The droplet was finally cooled to the final temperature to advance its freezing. This protocol reproduces the sequence of events expected during slow experimental cooling. In contrast, the fast-cooling protocol consisted of direct cooling from 350 K to 278 K, resulting in nearly simultaneous crystallization of the droplet surface and the drop interior.

Temperature and pressure are controlled using the velocity-rescaling (v-rescale) thermostat [46] and the Berendsen barostat [47], respectively. Pressure coupling is isotropically maintained at 1 bar. The respective contact times are 0.1 ps and 0.8 ps. The Berendsen barostat was employed to ensure methodological consistency with our previous simulations of related systems [39-42], thereby enabling direct comparison of the obtained structural results. Van der Waals interactions are modeled using a Lennard-Jones potential truncated at 1.2 nm, with a switching function starting at 1.0 nm. Electrostatic interactions are calculated using the Particle Mesh Ewald (PME) method [48-50], with real-space interactions truncated at 1.2 nm and a switching function activated at 1.0

nm. A 2 fs time step is used and the equations of motion are integrated using the leap-frog algorithm. All bonds involving hydrogen atoms are constrained with the LINCS algorithm [51] while water geometries are fixed with SETTLE [52].

Trajectory data are saved every 200 ps. The CHARMM36 force field [53] is employed together with the TIP4P water model [54, 55], both validated in our earlier studies [39-42] and shown to reproduce experimental data accurately.

All molecular dynamics simulations are performed using GROMACS 2021 [56], visualization is carried out with VMD 1.9.4 [57] and PyMOL [58]. Data analysis is performed using built-in GROMACS tools and custom analysis scripts developed in-house [39] (see the SI for details).

Results and Discussion

Kinetics of crystallization

As a first step in the analysis of the crystallization process of hexadecane, we investigated the freezing kinetics of the systems upon fast and slow freezing. To determine the fraction of frozen molecules, the distance between the third and thirteenth carbon atoms (Figure S1) along the hexadecane chain was calculated for each molecule in every simulation frame. A molecule was classified as frozen when the C3–C13 distance was ≥ 1.25 nm, corresponding to the fully extended *all-trans* conformation of this segment of the alkane chain. The results presented in Figure 2A show a clear difference in the crystallization kinetics between the two freezing protocols. The system subjected to slow freezing reaches a higher fraction of frozen molecules compared to the rapidly cooled system. This behavior is most likely related to the longer relaxation time available during slow freezing, which allows the molecules to rearrange more efficiently and adopt more favorable packing configurations.

It is also evident that in both systems the crystallization process has not been fully completed, as indicated by the remaining, albeit small, slope of the curves. Approximately 15% of the molecules still do not satisfy the criteria for frozen molecules. These molecules rearrange and reorient very slowly because they are typically trapped in structural defects or voids between crystallites. Their incorporation into the crystalline domains requires cooperative molecular rearrangements and the disruption of the local packing, making this process kinetically slow. Consequently, the final stage of structural relaxation proceeds over very long timescales. The simulations were therefore not extended further, as additional sampling would provide only marginal benefits for the interpretation of the results and the overall conclusions.

To further examine the observed crystallization kinetics and determine which type of molecules primarily contributes to the process, an additional analysis was performed (Figure 2B).

There, the number of frozen molecules is shown as a function of time for the two molecular species (hexadecane and surfactant).

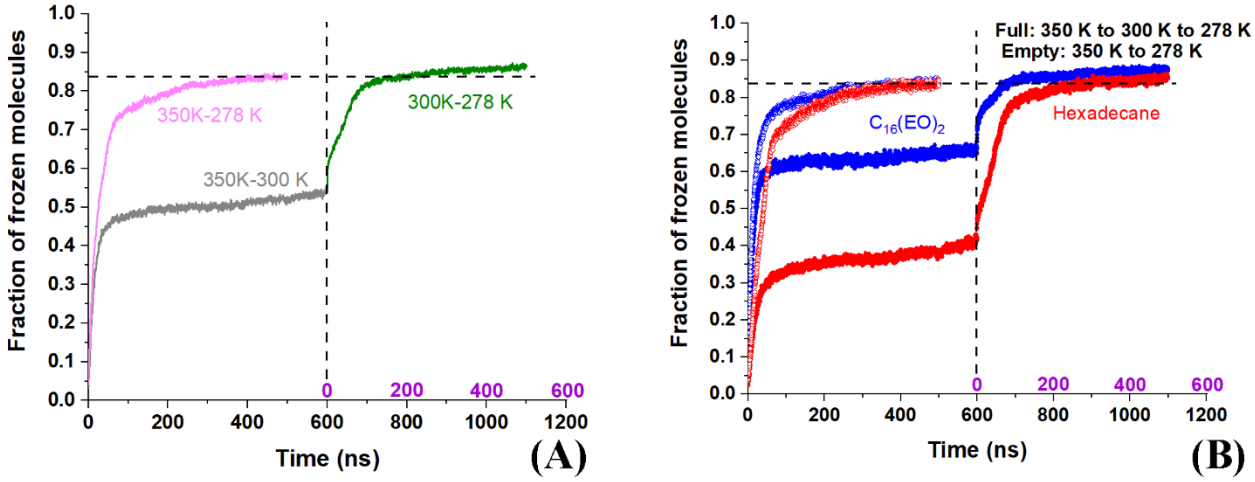

Figure 2. Fraction of frozen molecules as a function of time: (A) for the entire system, slow freezing (gray: 300 K; green: 278 K) and fast freezing (pink) and (B) shown separately for alkane molecules (red) and surfactant molecules (blue). The fractions are normalized to the total number of molecules of the respective type for both freezing protocols.

For the system subjected to slow freezing, during the first stage of cooling down to 300 K, approximately 65% of the surfactant molecules freeze, while only about 35% of the hexadecane molecules satisfy the freezing criterion. During the second stage, upon further cooling to 278 K, additional ~20% of the surfactant molecules and ~50% of the hexadecane molecules freeze. This behavior suggests that in the first stage the frozen molecules are primarily associated with the droplet surface, whereas in the second stage crystallization proceeds mainly in the droplet interior.

In contrast, in the fast freezing from 350 K directly to 278 K the curves for hexadecane and surfactant molecules almost overlap. A slight shift in the hexadecane curve is observed, which is likely related to the fact that the surfactant molecules freeze somewhat earlier. The shape of the curves indicates that, under fast freezing, the crystallization of the surface layer and the droplet interior occurs simultaneously.

To verify these varying mechanisms, a time-average radial analysis of frozen molecules was performed as a function of the distance from the droplet center. Figure 3 presents heatmaps for the two temperature regimes: the two stages of the slow freezing — the production simulation at 300 K (after cooling from 350 K) and at 278 K (after cooling from 300 K) — as well as the production simulation at 278 K for the fast freezing (after cooling from 350 K).

At 300 K (Figure 3A), the periphery of the droplet is already frozen, while the droplet interior remains liquid. It is also evident that the surface freezes almost immediately, whereas a

slight delay is observed in the subsurface region. The heatmaps clearly show that the droplet surface is composed predominantly of frozen surfactant molecules (shown in blue), while the subsurface layer consists mainly of frozen hexadecane molecules (shown in red). Upon further cooling of this system to 278 K, freezing gradually progresses deeper into the droplet interior, indicating that crystallization propagates from the surface toward the center of the droplet. For the fast freezing, the surface again freezes first. However, the subsequent crystallization occurs almost simultaneously throughout the entire droplet volume.

This analysis reveals clear differences in the crystallization behavior between the two freezing protocols, while consistently showing that surface freezing precedes bulk crystallization of the hexadecane droplet. Such behavior has also been observed experimentally [43, 59]. Previous studies have demonstrated that the surfactant plays a significant role in surface freezing and strongly influences the subsequent crystallization mechanism within the droplet interior [36, 37].

Therefore, the next important step was to examine the composition of the droplet surface and to determine whether it changes after the surface layer forms and freezes.

Effect of temperature on the redistribution and final composition of alkane and surfactant at the drop surface and in the drop interior

The number of frozen molecules of each type at the droplet surface and in the droplet interior for the two temperature regimes are summarized in Table 1. The number of surfactant molecules at the surface is higher at 300 K. However, the number of hexadecane molecules at the surface is also higher under these conditions. To allow a more meaningful comparison of the surface composition, the ratio between the number of surfactant and hexadecane molecules is calculated. The results show a noticeable difference between the two freezing protocols. For the system subjected to slow freezing, the surfactant-to-alkane ratio at the surface in the final frame of the trajectory at 278 K is 1.9, whereas for the rapidly cooled system it is 2.1.

To verify whether these differences could arise from fluctuations related to the dynamic nature of the interface, where adsorption and desorption processes may still occur even after surface freezing, the system is analyzed every 100 ns and block averages are calculated. The results show that the mean values remain statistically different within the standard deviations, 1.9±0.0 and 2.1, ±0.1 respectively, see Table 1.

It is also important to note that the surface of the slowly frozen system contains 293 more molecules in total (112 surfactant and 181 hexadecane molecules) compared to the rapidly crystallized one. This difference, as well as the different surfactant-to-alkane ratios at the interface, is most likely related to the different relaxation times available for surface restructuring. In the slow freezing, the system has approximately 600 ns to form and reorganize the surface before the droplet

interior undergoes a phase transition. Moreover, this occurs at the relatively higher temperature of 300 K, where molecular mobility is greater and rearrangements are easier.

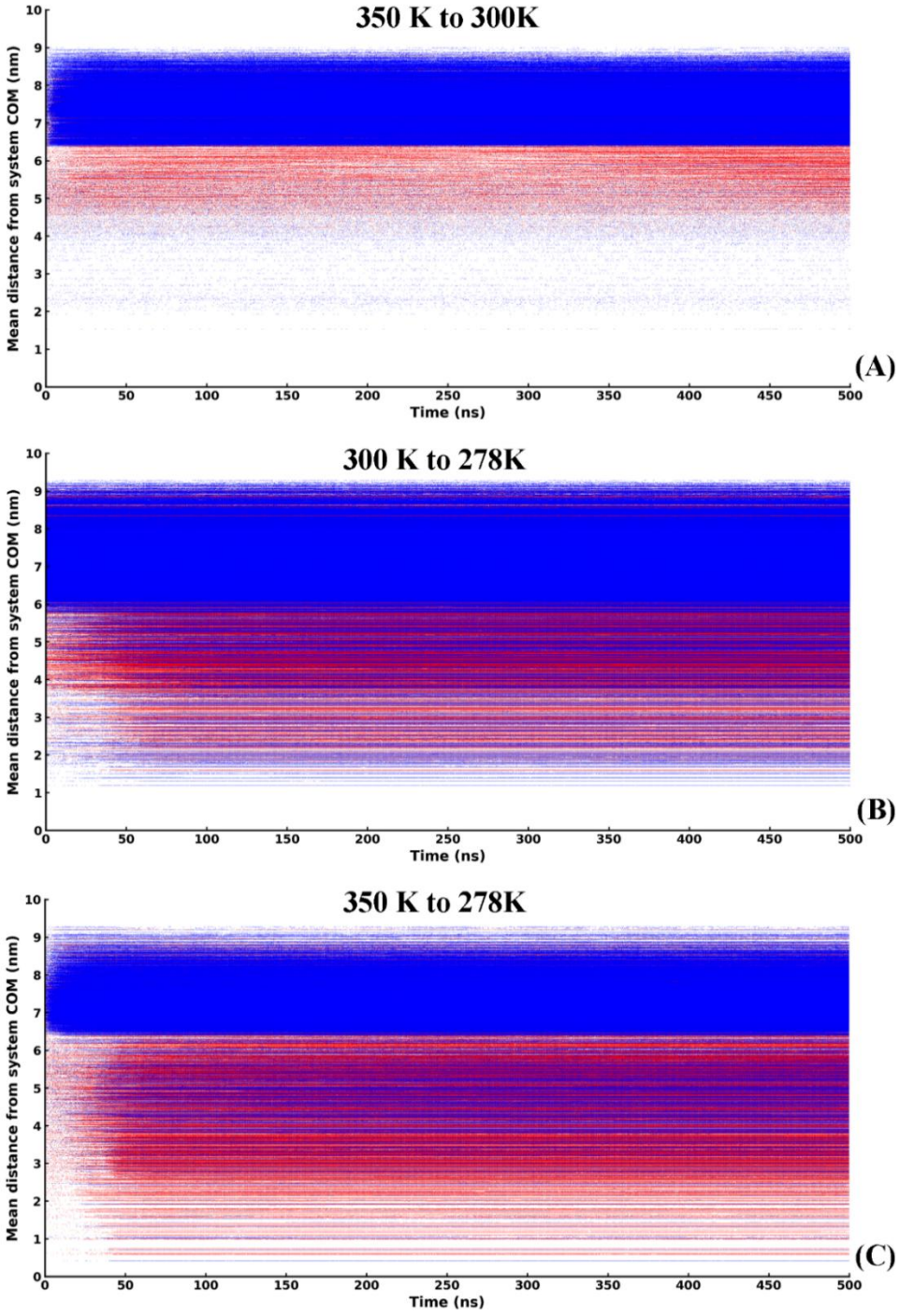

Figure 3. Heatmaps corresponding to the three production simulation stages: (A) at 300 K (after cooling from 350 K), (B) at 278 K (after cooling from 300 K), and (C) at 278 K (after cooling from 350 K). The heatmaps include only molecules classified as frozen. Frozen surfactant molecules are shown in blue and frozen hexadecane molecules – in red.

Comparison of the two stages of the slow freezing shows that once the surface layer is formed, its composition remains approximately constant despite the presence of interfacial dynamics and ongoing adsorption-desorption processes. This suggests that the observed composition represents a near-equilibrium and energetically favorable surfactant-to-alkane ratio for this system.

Table 1. Number of surfactant and hexadecane molecules at the surface and in the bulk; mean values with standard deviations from block averaging are summarized

	300 K		**278 K (from 300 K)**		**278 K (from 350 K)**	
	Core	**Shell**	**Core**	**Shell**	**Core**	**Shell**
$C_{16}EO_2$	993±21	2007±21	543±14	2458±14	654±66	2346±66
HEX	1768±19	1023±19	1484±24	1307±24	1665±43	1126±43
$C_{16}EO_2$/HEX ratio	**0.4±0.0**	**2.0±0.0**	**0.4±0.0**	**1.9±0.0**	**0.4±0.0**	**2.1±0.1**

In contrast, in the fast-freezing regime crystallization of the surface and the droplet interior occurs almost simultaneously. As a result, the surface has less time to reorganize, and the lower temperature further reduces molecular mobility, making molecular reorientation slower and more difficult. These observations clearly indicate that the freezing protocol plays an important role not only in determining the surface composition but also in controlling the packing efficiency of the molecules at the droplet interface. The importance of the cooling rate has also been clearly demonstrated experimentally [43].

Although the specific numerical values reported here are system-dependent and should not be regarded as universal, the influence of the cooling rate on molecular ordering and the resulting crystal structures represent a much more general phenomenon. This qualitative trend is fully consistent with the available experimental data [43].

Freezing mechanism

Since the cooling protocol plays an important role in both the crystallization kinetics and the surface composition, the next logical step is to investigate the crystallization mechanism under the two temperature regimes and to determine whether there are differences as well.

As already observed from the kinetics of the number of frozen molecules, the droplet surface freezes first under both cooling regimes. The first question we address is how crystallization

at the surface begins: whether it starts from a single nucleus that subsequently grows and spreads along the surface, or multiple nuclei form simultaneously.

Figure 4A presents snapshots of the initial stages of crystallization for both temperature regimes. It is clearly seen that crystallization of the $C_{16}(EO)_2$/hexadecane droplet starts simultaneously from multiple independent nuclei distributed along the droplet surface. In all cases, the first ordered molecules are surfactant molecules, which subsequently serve as templates for the ordering of additional surfactant, as well as hexadecane molecules.

From a mechanistic point of view, the crystallization process starts via the rapid formation of numerous independent surface nuclei separated by fluid regions. These nuclei subsequently grow, as additional molecules incorporate into the ordered structures. When two growing crystallites meet, two scenarios are observed: they either merge into a larger crystallite or remain separated by a defect region.

The next step was to examine how crystallization starts in the droplet interior and whether the frozen surface induces crystallization in the bulk. Figures 4B and 4C show snapshots illustrating the formation of the first crystallites in the droplet interior for the two freezing regimes.

For the slow freezing (Figure 4B), one crystallite forms already at 300 K, directly beneath the surface. After 4 ns, two independent crystallites appear, which subsequently merge into a single larger crystallite. Additional crystallites appear at 8 ns, 12 ns, and 20 ns. These crystallites form independently and are typically located close to the droplet surface.

In the fast freezing (Figure 4C), four crystallites appear almost simultaneously. Two of them later merge into a larger crystallite that eventually spans the entire droplet. Additional crystallites appear at 36 ns and 40 ns. As in the slow freezing, crystallites form independently and most often originate close to the droplet surface. The crystallites also exhibit different orientations with respect to the surface, which will be discussed in more detail in the following section.

It is important to note that crystallization in the droplet interior always starts from surfactant molecules, regardless of the cooling regime. This phenomenon has also been observed in our previous simulations [40-42], which indicates that the surfactant plays a crucial role by acting as a nucleation site for crystallization. In other words, the crystallization process advances through heterogeneous nucleation induced by the surfactant molecules.

This interpretation is consistent also with our previous simulations of surfactant-free alkane systems [40], in which crystallization proceeds via homogeneous nucleation, whereas in surfactant-stabilized droplets nucleation consistently initiates at the surfactant-covered interface.

Another important observation is the deformation of the droplet during the slow freezing. Such deformation has also been reported experimentally and is commonly associated with the formation of rotator phases [45, 60]. Experimental studies suggest that surface freezing takes place first and that the subsequent deformation of the droplet requires the formation of multilayers of a

plastic rotator phase [61]. A single molecular layer is generally considered insufficient to overcome the capillary pressure that maintains the spherical shape of the droplet.

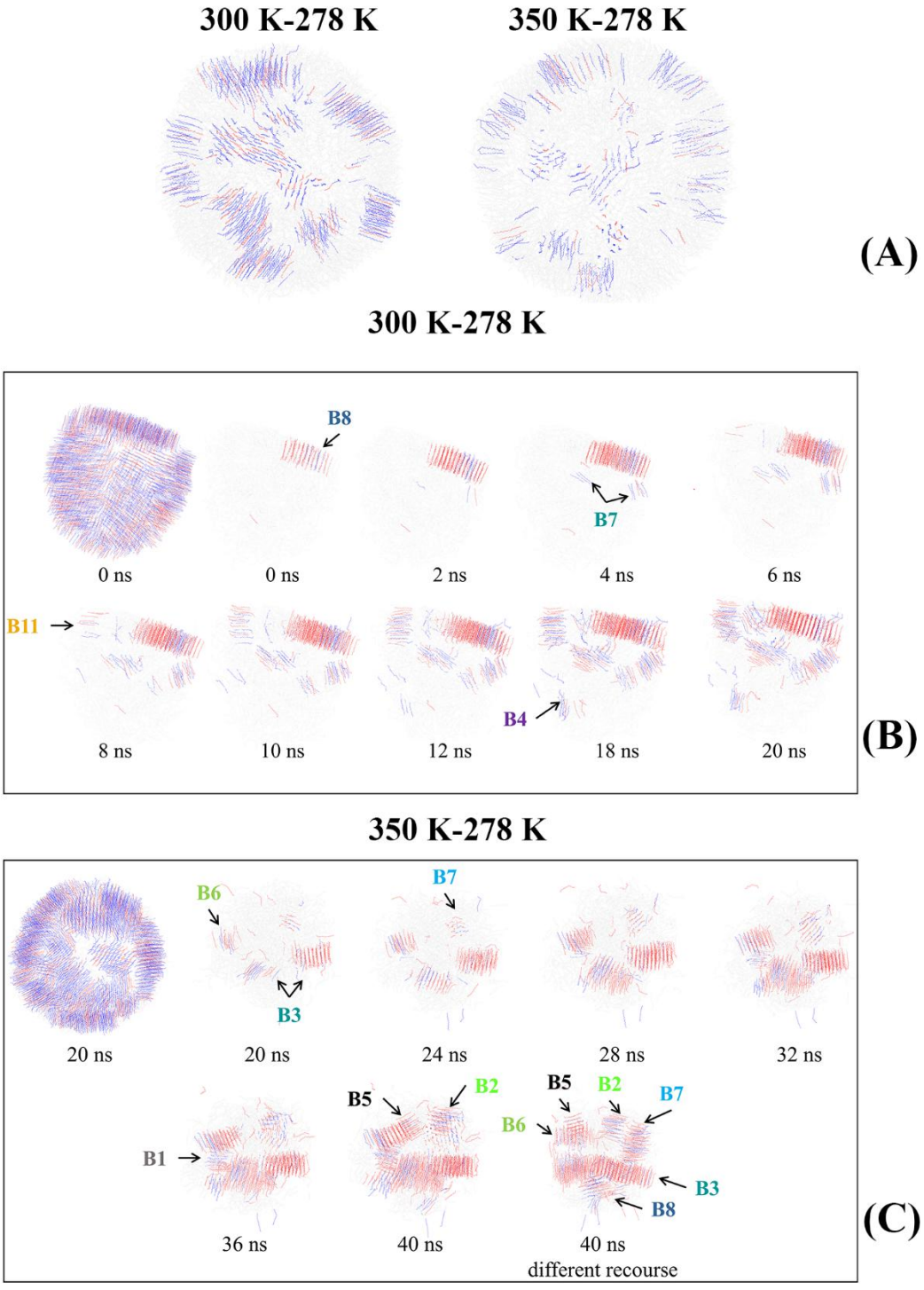

Figure 4. Snapshots illustrating the initial stages of crystallization: (A) on the droplets surfaces, (B) in the droplet interior for the system subjected to slow freezing, and (C) in the droplet interior

for the system subjected to fast freezing. Surfactant molecules are shown in blue, hexadecane molecules – in red. Bulk crystallites are labeled B# and correspond to the crystallites shown in Figure 5.

However, in our simulations, droplet deformation is observed already when only the surface layer is frozen, while the droplet interior remains liquid (with the exception of the early crystallite forming beneath the surface). This suggests that in nanoscale droplets a single ordered surface layer may already be sufficient to induce deformation.

One possible explanation for this discrepancy is the much higher surface-to-volume ratio in the smaller nanodroplets simulated in the current study. Experimental droplets typically have diameters of the order of micrometers, whereas in the present study the droplet diameter is 15 nm. The bending elasticity required to overcome the capillary pressure $K_B \geq \gamma r^2$ where γ is the oil-water interfacial tension (γ = 2 to 10 mN/m is taken in this study as a typical value [43]) and r is the droplet radius. For micrometer-sized droplets, this ratio yields values of approximately 10^{-15} to 10^{-14} J, which are several orders of magnitude larger than the bending constant of frozen surfactant monolayers 10^{-18} to 10^{-17} J [45,62, 63, 64,65]. In contrast, for nanometer-sized droplets, such as those studied here, the required bending constant is significantly smaller: 10^{-19} to 10^{-18} J. Therefore, while multilayers of plastic rotator phase may be necessary to deform micrometer-sized droplets, in nanoscale droplets the formation of a single ordered surface layer should already be sufficient to induce deformation, as shown also experimentally [45]. Based on these general considerations, the single-layer deformation effect should be valid also for such small oil droplets with different alkane/surfactant compositions.

As a next step, we investigated the crystallization mechanism in more detail. In particular, we determine the orientations of the different crystallites, the origin of each crystallite, the shape of the droplet surface, and the number of crystallites or surface planes forming the droplet shape. To perform this analysis, it was necessary first to determine the number of crystallites present in each system and identify which molecules belong to a given crystallite.

Figure 5A and B present snapshots from the final frame of the simulations for the two temperature regimes. In the first row of both panels, the crystallites forming the droplet surface are shown and labeled as S followed by a number, while the crystallites located in the droplet interior are shown below and labeled as B followed by a number. It can be clearly seen that in both droplets the surface consists of five crystal planes, which define the final droplet shape.

For the slow cooling protocol, 12 crystallites are present in the $C_{16}(EO)_2$/hexadecane droplet interior at the end of the simulation, whereas only 8 crystallites are observed after fast cooling. While these numbers are specific to the present system, they illustrate a more general difference in crystallization kinetics. Fast cooling produces many nuclei within a short time interval, leading to early impingement between growing crystallites, which restricts subsequent nucleation, growth, and structural reorganization. Under slow cooling, nucleation is spread over longer time, allowing

additional crystallites to develop before impingement occurs. Consequently, the final number of crystallites is higher for the slow cooling protocol.

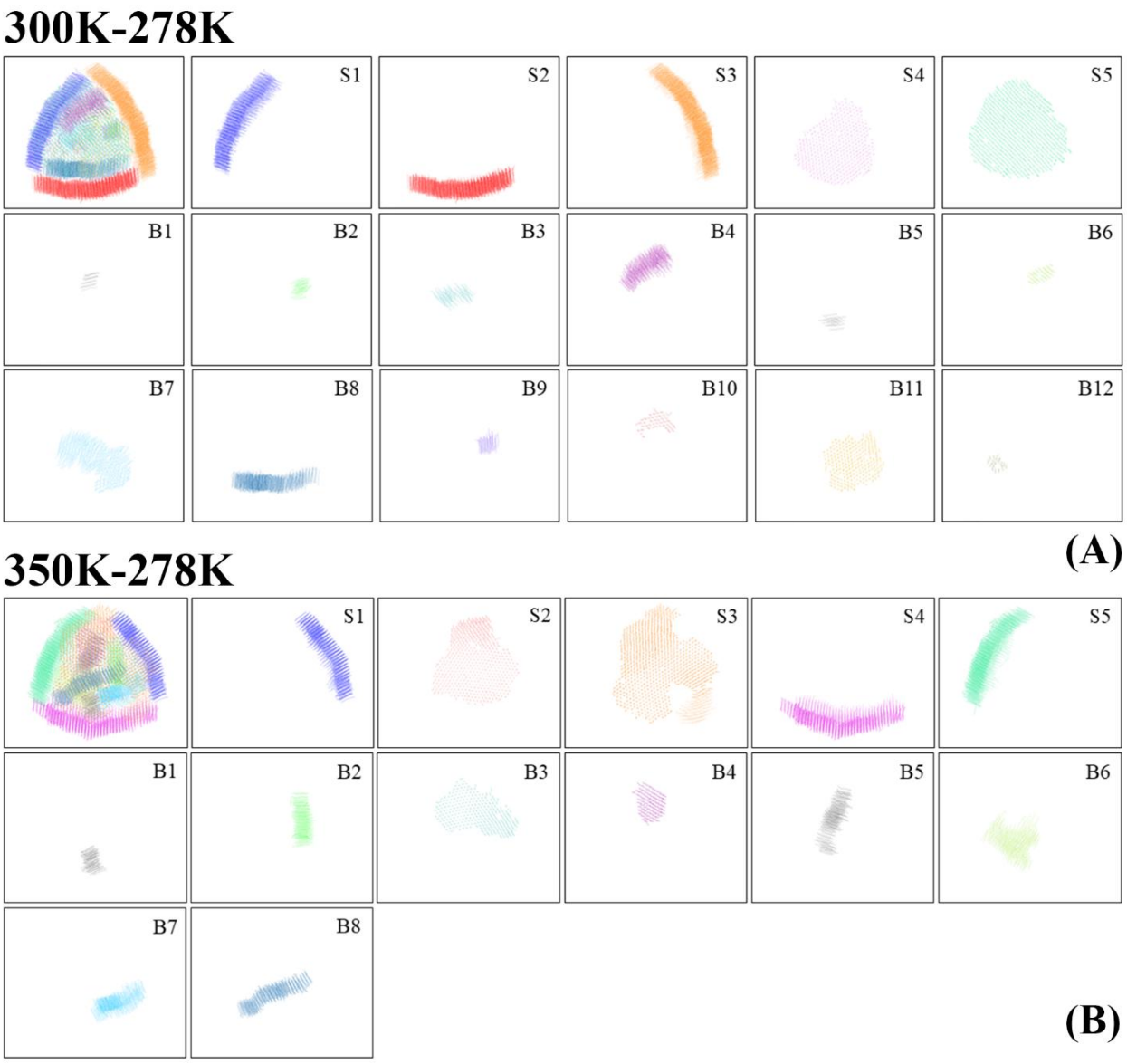

Figure 5. Snapshots of the final frame illustrating all crystallites: (A) slow freezing and (B) fast freezing. Surface crystallites (top) are labeled S#, and bulk crystallites (bottom) B#. Each crystallite is assigned a unique color, consistently used throughout all subsequent figures.

The variation from rod-like to plate-like crystallite morphologies is attributed to directional growth constraints imposed by neighboring crystallites. Blocking of lateral growth favors elongation into a narrow rod-like structure, whereas restriction of longitudinal growth, while lateral expansion remains possible, results in a broader plate-like morphology.

Both droplets exhibit a triangular prism-like shape, although the droplet obtained with the slow freezing has a more regular geometry and smoother surfaces. This observation is consistent with the longer relaxation time available for the formation and reorganization of the surface before crystallization begins in the droplet interior. It is shown experimentally that the final droplet morphology depends on the surfactant, alkane, and cooling rate. For the $C_{16}EO_2$/hexadecane system investigated here, our previous experimental studies report polyhedral particles [43, 45]. Although some surfactant/alkane systems may evolve into rod-like or fibrous morphologies, such transformations occur under much slower cooling conditions than those accessible by atomistic molecular dynamics simulations. Therefore, the polyhedral morphology observed here is consistent with the experimental observations for this system and the timescale limitations of the simulations, which reveal only the initial shapes formed upon freezing.

After determining the number of crystallites in each system, we analyzed the number of droplet surfaces in contact with each bulk crystallite in the final configuration. It should be noted that contact with a surface does not necessarily imply that the crystallite nucleated at the surface; it may also nucleate in the interior and later grow until it touches one or several surfaces.

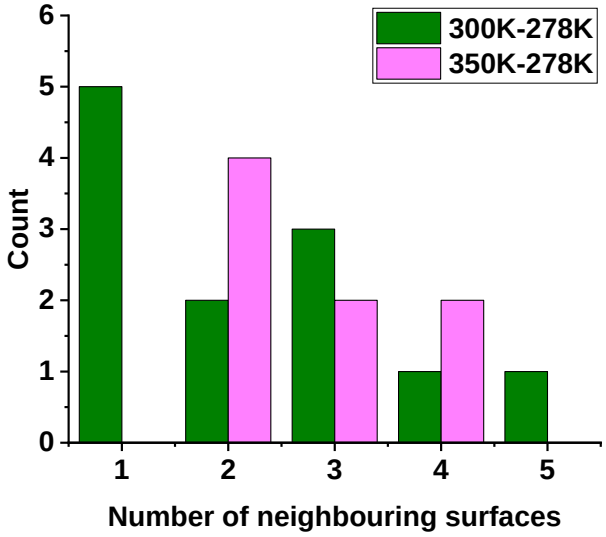

Figure 6. Histogram of the number of neighboring surface planes per crystallite: slow freezing (green) and fast freezing (pink).

Figure 6 summarizes the number of neighboring surfaces in contact with each bulk crystallite formed in the two simulated droplets. Owing to the limited number of crystallites, these data should be interpreted as a qualitative comparison rather than a statistically representative distribution. In the slow-cooling simulation, crystallites most frequently contact a single neighboring surface, whereas contacts with three neighboring surfaces are less common, followed by contacts with two surfaces. Contacts with four or five neighboring surfaces are observed only occasionally. In

contrast, the fast-cooling simulation shows a different trend, with crystallites most frequently contacting two neighboring surfaces, while contacts with three or four neighboring surfaces occur less often. Notably, no crystallite in the fast-cooled system contacts a single neighboring surface, whereas this is the most common configuration in the slow-cooled system. This qualitative difference is consistent with the more simultaneous growth and earlier impingement of crystallites during rapid cooling.

The number of surfaces in contact with a crystallite can correspond to several possible geometric configurations. A crystallite contacting one surface may either terminate within the droplet interior or grow along the surface without reaching its edges. If a crystallite contacts two surfaces, several configurations are possible: it may grow along a surface and reach one of its edges, it may be oriented along the boundary between two surfaces, or it may span the entire droplet and contact two opposite surfaces. For three adjacent surfaces, the crystallite may extend along one surface and reach both of its edges, nucleate near the intersection of three surfaces (at the frozen droplet vertices), or contact one surface and an adjacent edge. Crystallites contacting four or five surfaces typically involve intersections with edges and often extend across the droplet toward an opposite surface.

The presence of crystallites contacting multiple surfaces and the occurrence of higher numbers of neighboring surfaces (four or five) suggest that the crystallites in the droplet interior adopt a wide range of orientations. These crystallites appear to support the droplet surfaces in a scaffold-like manner, which could contribute to the stabilization of the observed droplet deformation.

To further clarify the crystallization mechanism and determine whether the droplet surface induces crystallization in the interior, as well as to quantify the mutual orientation of crystallites, additional analyses were performed.

As a first step, we determined the angles between the planes of pairs of surface crystallites. The angle between two crystallites was defined as the angle between the normal vectors of the best-fit planes calculated for each crystallite. The plane-fitting procedure is described in detail in Ref. [39]. The reported values correspond to time-averaged angles. The results are summarized in Table 2. For the slow freezing, the surfaces that do not share a boundary are surfaces 4 and 5, which are positioned opposite each other. In the fast-freezing case, the opposite surfaces are 2 and 3. In both systems, these opposite planes are nearly parallel, forming small angles (up to 30°) with respect to each other. The deviation from perfect parallelism is slightly larger for the fast freezing, most likely due to the shorter relaxation time available for surface restructuring.

The remaining surface pairs form significantly larger angles, which in most cases are either close to 60° or to 90°, indicating that the drop shape resembles that of a vertical prism with triangular bases. This configuration implies that the surfaces intersect rather than bend

continuously. Such an arrangement explains how the droplet can form sharp edges without requiring large bending energies that would normally be associated with highly curved interfaces. Instead, the studied system achieves this geometry through the intersection of nearly planar surface domains, thus avoiding large energetic penalties.

Table 2. Angles between pairs of surface planes. Values for non-adjacent (opposite) faces are highlighted in brown.

300K->278K					
Surface	**Surface**				
	1	**2**	**3**	**4**	**5**
1	--	56.9±0.4	56.7±0.4	75.5±0.6	86.8±0.5
2		--	68.9±0.4	88.5±0.4	77.7±0.4
3			--	88.6±0.5	82.5±0.4
4				--	18.3±0.5
5					--
350K->278K					
	1	**2**	**3**	**4**	**5**
1	--	71.5 ±0.9	84.7 ±0.7	60.5 ±0.5	53.8 ±0.5
2		--	30.2 ±0.5	85.8 ±0.5	89.1 ±0.5
3			--	66.1 ±0.4	89.5 ±0.4
4				--	68.7 ±0.3
5					--

A few smaller angles between surfaces are also observed, which are most likely related to the system adjusting toward an energetically favorable overall droplet shape. Despite the fact that the surfaces appear somewhat rougher and less regular in the rapidly frozen system, the overall droplet geometry obtained under both cooling protocols is essentially the same. This result suggests that the observed shape represents a preferred equilibrium morphology for this system.

Experimentally, regular droplet shapes have been reported, together with subsequent transformations into other morphologies during further evolution of the system [43]. In the present simulations, however, no such additional transformations are observed. This is most likely due to the relatively short simulation time, combined with fast cooling protocols, compared to experimental conditions, where longer observation times and slower cooling rates allow the system to evolve further along the morphological transformation pathways.

The next step was to determine whether the droplet surface induces crystallization in the droplet interior. To address this question, we performed a detailed analysis of all crystallites that

were found to be in contact with a given surface. Using visual inspection of the trajectories, we determined whether each crystallite originated from the respective surface. For crystallites contacting more than one surface, this analysis was performed for each surface pair.

Figures 7A and 7B show each surface together with the bulk crystallites originating from it. For the slow freezing (Figure 7A), the two crystallites stemming from surface S1 grow almost perpendicular to it, whereas for S2 configurations parallel to the surface are also observed. For surface S5, orientations corresponding to angles different from those close to 0° or 90° are also possible. A similar behavior is observed for the fast freezing.

Nevertheless, visual inspection of the snapshots suggests that crystallites preferentially adopt orientations close to perpendicular to the droplet surface. To further examine this observation, histograms of the crystallite orientation angles were constructed for both systems (Figure 7C). Although based on a limited number of crystallites, the data consistently indicate that orientations above approximately 70° are the most frequently observed, whereas smaller orientation angles occur considerably less often.

An interesting qualitative difference between the two cooling protocols is that, in the slow-cooling simulation, crystallites with orientation angles between 0° and approximately 60° are also observed, while such configurations are very few under fast-cooling conditions. The occurrence of smaller orientation angles during slow cooling may be promoted by the better ordering of the surface layer. In contrast, the less ordered and rougher surface formed during fast cooling may suppress crystallite orientations closer to parallel with the droplet surface. Overall, the present simulations suggest that orientations close to perpendicular to the droplet surface are favored, whereas parallel or near-parallel orientations appear only under specific crystallization conditions. This observation contrasts with the commonly assumed preferential parallel alignment invoked in some proposed mechanisms of droplet deformation [43] and is consistent with previous studies suggesting that crystallites may adopt orientations closer to perpendicular to the droplet surface [37].

The values of the angles for each pair of crystallites, together with the corresponding standard deviations, calculated over the last 100 ns of the simulations, are presented in Table S1. The standard deviations are relatively small, indicating that the orientations of the crystallites remain stable over time. This stability is most likely related to the fact that the crystallites interlock with one another, forming a mechanically robust, rod-like network. Such an intertwined structure effectively acts as a scaffold, which further contributes to the stabilization of the $C_{16}(EO)_2$/hexadecane droplet shape.

In our analysis, we found for both systems that only one crystallite nucleates in the bulk (8.3 % for slow and 12.5 % for fast freezing), whereas all others originate at the surface. On the other hand, 50.0 % of the crystallites in the slow freezing and 62.5 % in the fast freezing nucleate

from a single surface, which is a similar probability in the framework of the stochastic process considered.

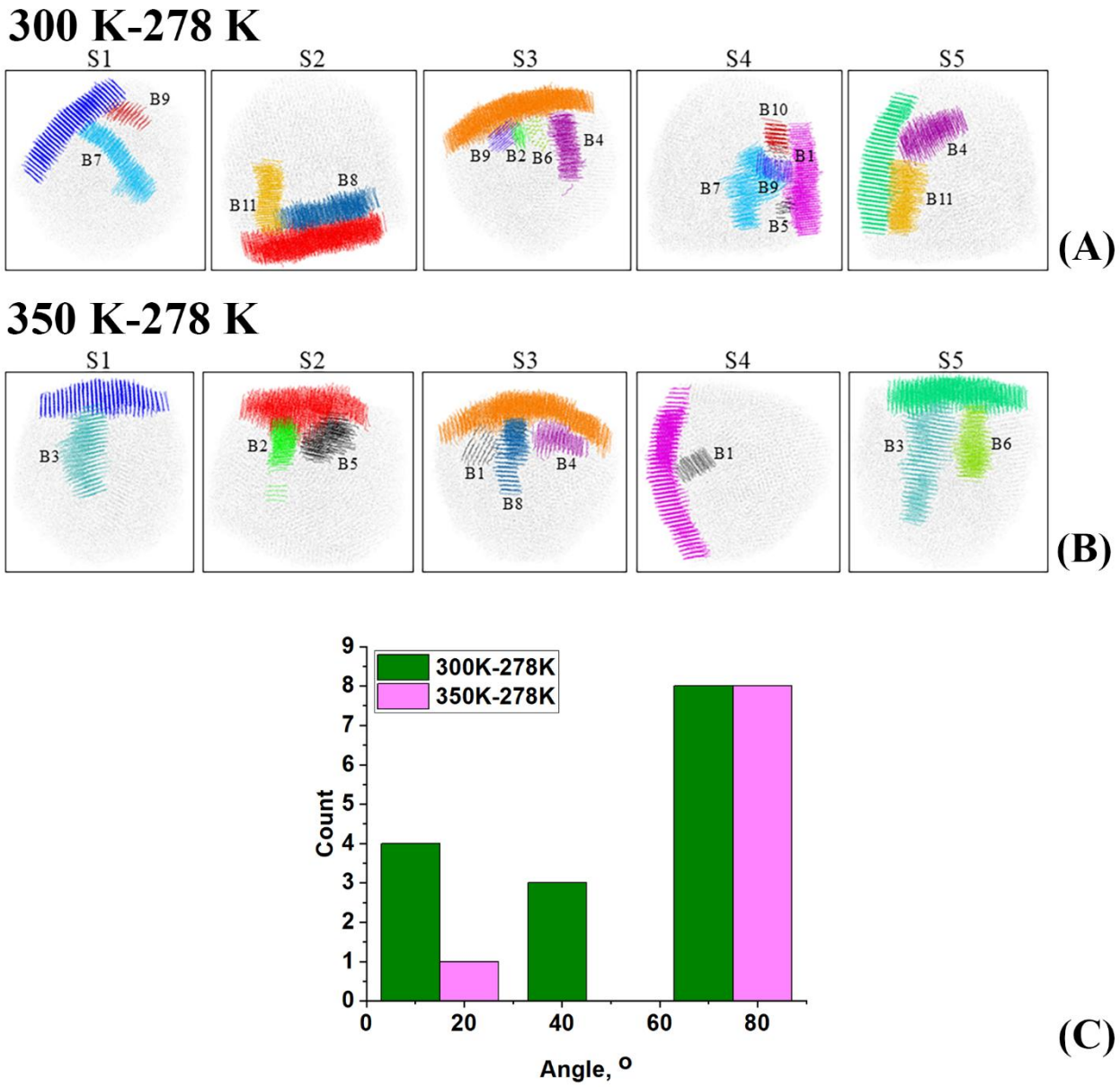

Figure 7. Angles between surface planes and the crystallites originating from them. (A, B) Final-frame snapshots showing crystallite orientations. (C) Angle distribution histogram: slow freezing (green) and fast freezing (pink).

It was also interesting to examine whether bulk crystallites could nucleate simultaneously from two neighboring surface crystallites. Our analysis shows that for the system subjected to the slow freezing, five crystallites (approximately 41.7 % of the bulk crystallites) originate from the

edge between two surface planes. In contrast, for the fast freezing only two crystallites (about 25.0 % of the bulk crystallites) nucleate at such surface edges.

This difference may be related to the better ordering of the surface at 300 K in the slow freezing, which likely allows better molecular packing at the edges between surface planes and thus facilitates subsequent crystallization. In all such witnessed cases, however, it is evident that the edges between surface planes represent preferred nucleation sites. Most often, the crystallite originates perpendicular to one of the surfaces and grows along the other. This behavior may be attributed to the fact that edges possess different energetic characteristics compared to the planar regions of the surface, which can promote nucleation processes. This observation is consistent with classical nucleation concepts, according to which edges and surface irregularities often act as energetically favorable sites for heterogeneous nucleation due to the reduced free-energy barrier compared to flat surfaces [66, 67]. Sear et al. [67] have shown that defects forming perpendicular angles can have a significant effect on the crystallization barrier. Similar angular features are observed in the deformed droplets obtained in our simulations. On the other hand, these surface edges and the crystallites nucleated beneath them most likely play an important role in the subsequent droplet deformation and may influence the pathway along which the droplet evolves through the sequence of shapes observed experimentally [43].

As a side note, when two or more crystallites approach each other in the bulk, the most proximate molecules rearrange significantly to allow merging in a final larger crystallite.

After investigating the crystallization mechanism in detail, we next examined the type of phase formed in the different crystallites and whether it depends on the cooling protocol.

Crystallites phase state

In our previous studies [39-42], we have highlighted the fraction of *gauche* defects as a very sensitive parameter for distinguishing between the different phases (isotropic liquid, rotator phase, rotator to crystalline transition, and crystalline phase) in alkane-containing systems. Therefore, we analyzed the ratio of *gauche* defects for the entire drop as well as for each crystallite individually.

The kinetic curves of the *gauche* defect fraction as a function of time are shown in Figure 8. For the slow freezing, a slight decrease in the number of *gauche* defects is observed at the beginning of the simulation, from approximately 36 % to 26 %, which is most likely associated with the freezing of the droplet surface. However, since the droplet interior remains fluid, the overall fraction of *gauche* defects remains relatively high, close to values typical for a liquid phase. Upon further cooling, a sharp transition is observed. At approximately 670 ns, the rapid decrease stops and the system reaches a value of about 14 % *gauche* conformations, which is characteristic of a rotator phase [42].

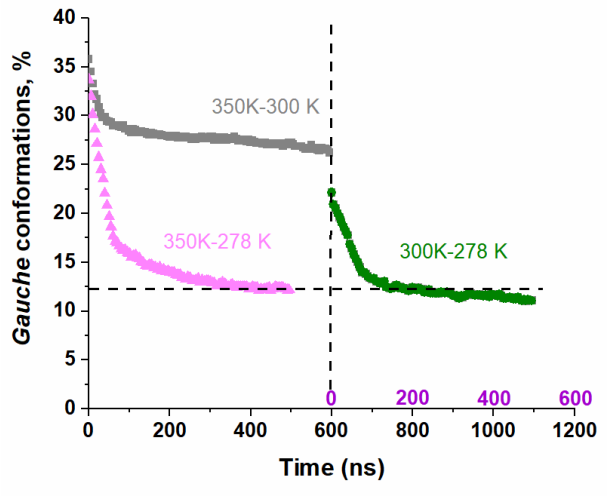

Figure 8. Fraction of *gauche* conformations as a function of time for the two freezing protocols: slow freezing (gray: 300 K; green: 278 K) and fast freezing (pink).

For the fast freezing, the kinetics is somewhat different. In the initial stage, a sharp decrease is observed again. However, the steep reduction ends around 65 ns, after which a much slower decrease is observed, starting from approximately 17 % *gauche* conformations. Throughout this gradual decrease, the values remain within the range typical for a rotator phase.

In both systems, the initial relaxation lasts for approximately 70 ns, after which a second stage follows with a milder slope and a duration that differs between the two freezing protocols. With both freezing protocols, a significant number of *gauche* defects remains at the end of the simulation (12 % for the 300–278 K protocol and 11 % for the 350–278 K protocol), indicating that the systems persist in a rotator phase.

This result is particularly important because it highlights the fundamental difference in the phase stability under micro- and nano-confinement compared to bulk systems. Experimental studies have shown that for bulk hexadecane only a transient rotator phase is observed, whereas under confinement (e.g., in pores) this phase becomes thermodynamically stable, being registered both during cooling and heating [26]. The results obtained here are therefore in very good agreement with the experimental observations [26, 36, 37].

To determine the phase of each crystallite individually and to examine whether significant differences exist in the fraction of *gauche* conformations (i.e., whether different crystallites are at different stages of crystallization), we analyzed the fraction of *gauche* defects separately for each crystallite.

The results (Table 3) show that the surface crystallites (surface planes) in both systems exhibit values between 5.3 % and 7.2 % *gauche* conformations. For the slow freezing, the crystallites feature lower values, with an average of 5.5 %, which is already close to the transition

toward a more ordered crystal state [42]. This result indicates that the system is further ahead along the crystallization pathway compared to the rapidly cooled system, for which the average value is 6.6 %. The mean values (5.5 ± 0.2 and 6.6 ± 0.5) are statistically different (two-tailed Student's t-test, n = 5, p = 0.01), which confirms the trends observed in the previous analyses.

Table 3. Percentage of *gauche* conformations evaluated individually for each crystallite.

Crystallite number	*Gauche, %*			
	300-278K		350-278K	
	Surface	Core	Surface	Core
1	5.5	8.8	7.2	12.0
2	5.3	8.2	6.5	10.5
3	5.5	10.2	6.5	7.4
4	5.9	9.2	6.8	8.7
5	5.5	7.9	5.7	10.7
6		10.7		7.6
7		7.7		8.9
8		7.3		10.2
9		10.9		
10		11.7		
11		7.7		
12		13.2		
Average	**5.5±0.2**	**9.4±1.9**	**6.6±0.5**	**9.5±1.6**

The bulk crystallites contain higher fractions of *gauche* defects in both systems, which is expected. On the one hand, bulk crystallites appear later in the crystallization process and, on the other hand, micro- and nano-confinement is known to stabilize the rotator phase [26, 36, 37]. Interestingly, no significant difference is observed in the average values of the bulk crystallites between the two systems. This observation further confirms the stabilizing effect of confinement on the rotator phase, independent on both the relaxation time and the degree of surface ordering.

Based on the fraction of *gauche* defects, the structures appear to be in a rotator phase. However, to verify whether the molecular ordering and structure indeed correspond to a rotator or crystalline phase, additional analyses were performed.

Rotation about the second principal axis

Specifically, we analyzed the P_2 order parameter and the radial distribution functions (RDFs) of the different crystallites formed both at the $C_{16}(EO)_2$/hexadecane droplet surface and in the droplet interior. These results were compared with those obtained for reference systems, namely, a model triclinic phase and a model rotator phase R_I (which rapidly transforms in bulk systems toward the triclinic phase and therefore represents an intermediate $R_I \rightarrow T$ structure) of hexadecane, both of which were studied and analyzed in detail in our previous work [40].

Figure 9 presents the P_2 Jaccard indexes (see SI for details) for all investigated crystallites with respect to the two reference model systems. As can be seen, both surface and bulk crystallites show better agreement with the rotator phase than with the triclinic phase.

A comparison of the surface crystallites for the two freezing protocols (Figure 9A and C) reveals notable differences. For the slow freezing, three crystallites reach values of approximately 0.7, one is around 0.6, and one exhibits very low indices. This is an indication of low similarity to either of the reference systems. In contrast, for the fast freezing, one surface crystallite is more similar to $R_I \rightarrow T$ transition, with a value exceeding 0.8, three exhibit values around 0.6, and again one crystallite shows low similarity indices.

It is instructive to relate these observations to the geometry of the droplet. For slow freezing, similar values are observed for the two bases and one lateral face of the triangular prism, while the remaining two faces show lower indices. For fast freezing, a similar trend is observed, with the two bases and one side showing comparable values, while the other two faces differ significantly—one being closer to the rotator phase, and the other with low indices.

Most of the bulk crystallites (Figure 9B and D) exhibit relatively low Jaccard indices with respect to both reference systems, although they remain closer to the rotator phase. Only a few crystallites show higher values— crystallite 8 in the slow freezing and crystallites 3 and 6 in the fast freezing. Crystallite 8 (slow freezing) starts to form early, already at 300 K, and is oriented parallel to the adjacent surface (S2) from which it originates. In contrast, crystallite 3 (fast freezing) nucleates at the edge between surfaces 1 and 5 and is oriented nearly perpendicular to them. This is also the only crystallite exhibiting comparable similarity to both the triclinic and rotator reference phases.

The relatively low Jaccard indices indicate that the crystallites do not closely match either reference structure. While this is expected for the triclinic phase, the moderate similarity to the rotator reference requires further consideration. A likely explanation lies in the nature of the reference system itself. The model rotator phase was constructed as an RI phase, which is unstable in bulk hexadecane and rapidly evolves toward the triclinic phase during equilibration [40]. Consequently, the reference configuration represents an intermediate RI→T structure rather than a fully developed rotator phase. In contrast, under confinement the rotator phase is expected to be stable [26, 36, 37], and the crystallites observed in the present study are therefore likely closer to

an ideal confined rotator phase than to the bulk RI→T reference structure. This difference is expected to reduce the absolute Jaccard indices. Therefore, the Jaccard analysis should be interpreted as a measure of relative structural similarity rather than as a strict phase assignment. Within this framework, all crystallites consistently exhibit greater similarity to the rotator reference than to the triclinic reference, supporting a predominantly rotator-like local structure.

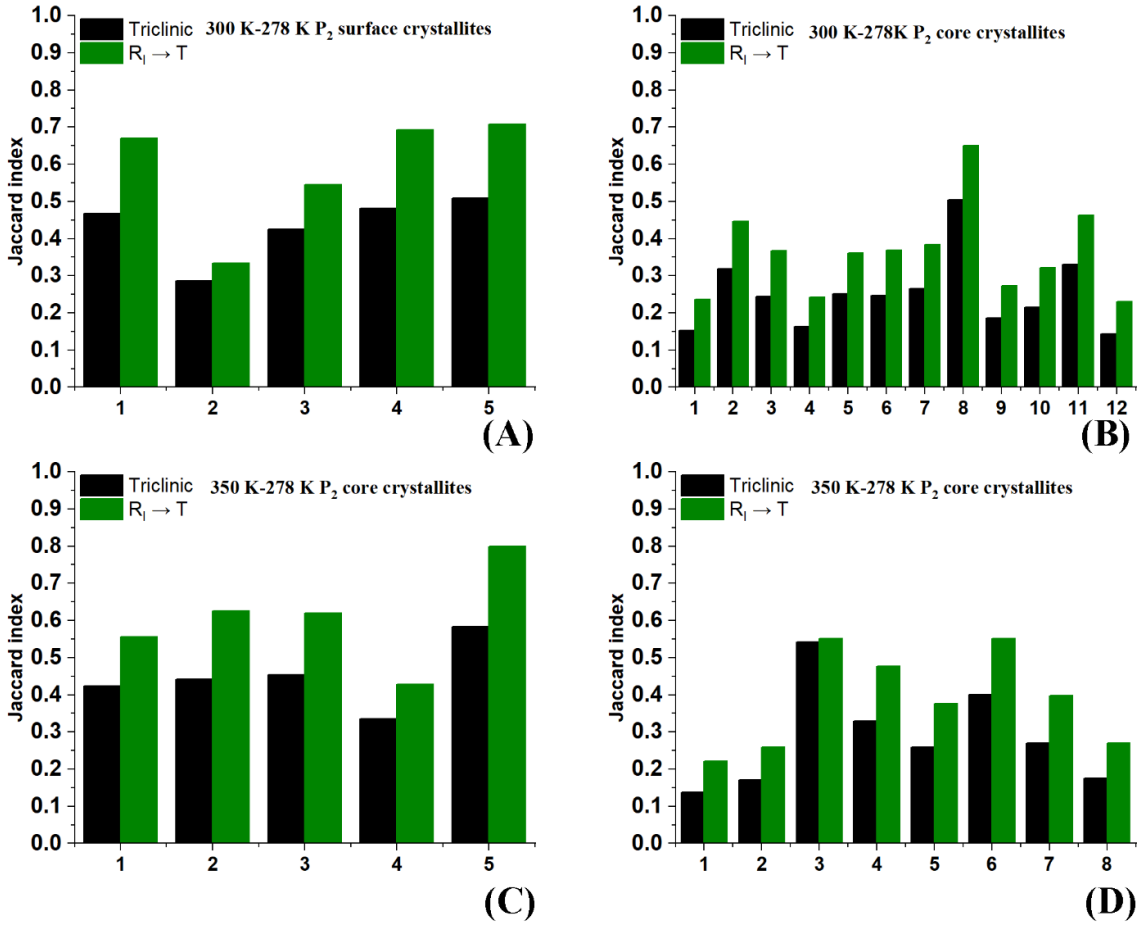

Figure 9. P_2 Jaccard indices quantifying the similarity of the model systems to the crystalline and rotator phases: (A) surface crystallites (slow freezing), (B) bulk crystallites (slow freezing), (C) surface crystallites (fast freezing), and (D) bulk crystallites (fast freezing). Data relative to the triclinic phase are shown in black, while those relative to the $R_I \rightarrow T$ transition are shown in green. The numbers on the abscissae are the crystallite numbers as introduced in Figure 5.

On the other hand, by examining the P_2 profiles of the individual crystallites (Figures S2–S5), it is possible to assess whether the structures correspond to a rotator or crystalline phase even without direct comparison to the reference systems.

From Figures S3 and S5, it is evident that most surface crystallites exhibit a similar profile, characterized by a central peak with broadened side lobes, the extent of which varies between crystallites. Notably, crystallite 2 (slow freezing) and crystallite 4 (fast freezing) display distinctly different profiles. A profile similar to that of crystallite 4 has been observed in our previous studies [40] and is typically associated with structural transformation or transition toward another phase. In contrast, the profile observed for crystallite 2 (slow freezing) is unusual: it shows comparable probabilities at 0° and +90°, and lower probability at −90°, which has not been observed previously in this form. Earlier, we have witnessed profiles with a dominant central peak at 0° and weaker satellite peaks around ±90°. The current profile most likely indicates the coexistence of two phases, whose preferred orientations are approximately perpendicular to each other.

Analysis of the bulk crystallites (Figures S2 and S4) shows that, although the profiles differ in terms of the number of peaks and their degree of broadening, most of them are characteristic of a rotator phase. The only exceptions are crystallite 8 (slow freezing) and crystallites 3 and 6 (fast freezing), which exhibit distinct profiles. This observation is consistent with the P_2 Jaccard indices: the higher similarity indices for these crystallites likely arise because they are more advanced along the crystallization pathway and are thus closer to the intermediate $R_I \rightarrow$ triclinic ($R_I \rightarrow T$) structure. In contrast, the remaining crystallites exhibit profiles typical of a rotator phase, which explains their lower similarity to the reference system, as they have not yet begun transitioning toward the triclinic phase.

Intermolecular packing assessed by radial distribution functions

A similar analysis was performed using the radial distribution functions in order to evaluate the structural similarity of the different crystallites with respect to the model reference systems.

As in the case of the P_2 analysis, the majority of crystallites exhibit higher similarity to the rotator phase than to the triclinic phase. However, the corresponding Jaccard indices are significantly higher (Figure 10). In particular, all surface crystallites show nearly identical indices, with values of approximately 0.7 relative to the rotator phase, Figure 10A and C. This result indicates that the molecular packing within these crystallites is closer to that of the rotator phase than to the triclinic structure and this conclusion is further confirmed by the individual RDF profiles of the different crystallites (Figures S7 and S9).

A similar trend is observed for the bulk crystallites, seven of which exhibit values around 0.7, indicating a high degree of structural similarity (Figures 10B, 10D, S6 and S8).

Overall, this analysis confirms that the majority of crystallites are in a rotator phase and possess a lattice resembling that of the model R_I phase.

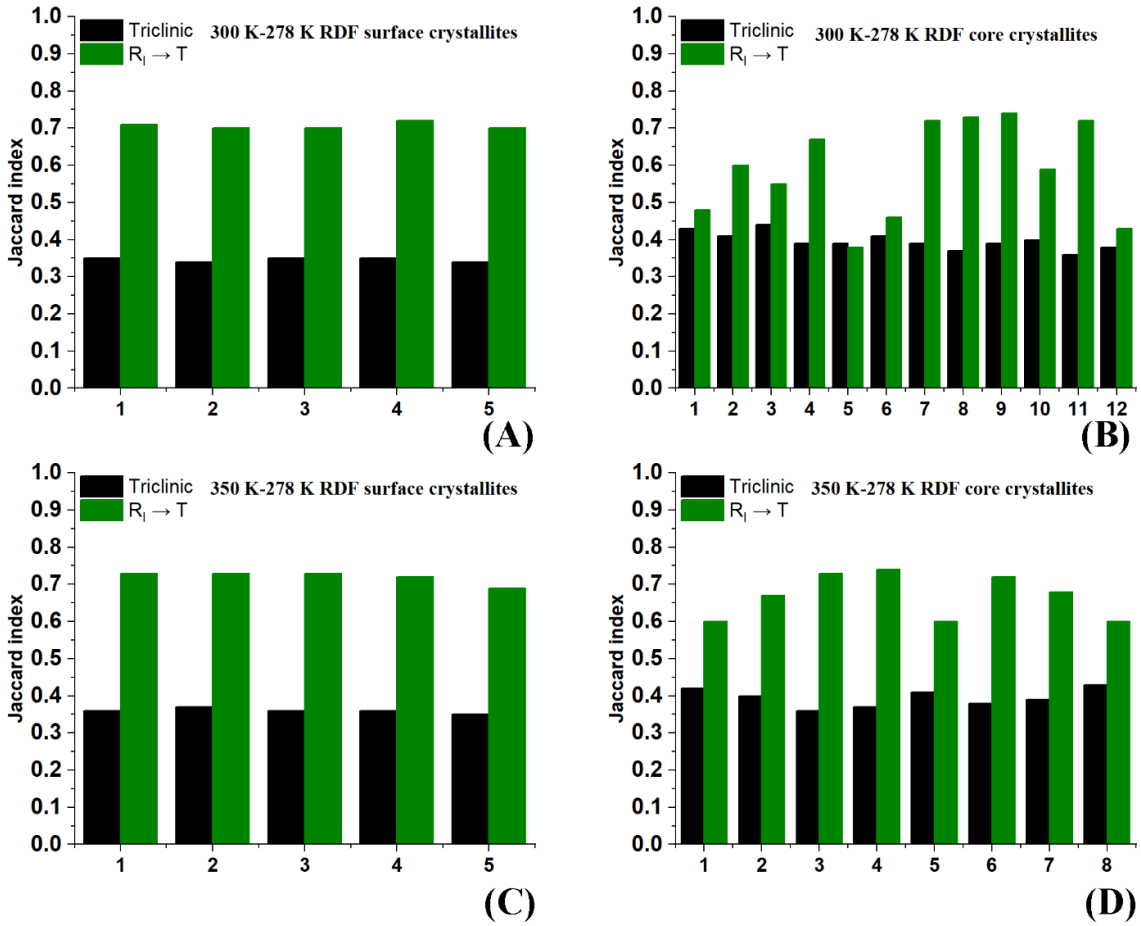

Figure 10. RDF Jaccard indices quantifying the similarity of the model systems to the crystalline and rotator phases: (A) surface crystallites (slow freezing), (B) bulk crystallites (slow freezing), (C) surface crystallites (fast freezing), and (D) bulk crystallites (fast freezing). Data relative to the triclinic phase are shown in black, while those relative to the $R_I \rightarrow T$ transition are shown in green. The numbers on the abscissae are the crystallite numbers as introduced in Figure 5.

Conclusions

The present work provides a detailed atomistic molecular dynamics investigation of the crystallization of surfactant-stabilized hexadecane droplets in water. A novel general procedure for spherical droplet construction is introduced, which enables controlled variation of the surface coverage with surfactant molecules. A model of ca. 2 000 000 atoms is simulated with two cooling protocols, employing a computational procedure developed in our previous studies [39-42], which may be generally applied to describe freezing phase transition in alkane-containing systems. Herein, the effect of spherical nano-confinement is traced.

In addition, the crystallization mechanism is elucidated in detail at the molecular level. Crystallization is found to initiate stochastically along the entire droplet surface, through the

formation of multiple independent nuclei, followed by crystallization in the droplet interior. Under a slow freezing protocol, a larger fraction of the system reaches the solid state, with crystallization progressing from the surface toward the drop center. In contrast, under fast freezing, a somewhat higher fraction of molecules remains disordered, as they become trapped between growing crystallites, hindering their rearrangement. In this case, crystallization occurs almost simultaneously throughout the droplet volume.

The surface composition depends on the freezing protocol, due to differences in the relaxation time, with the rapidly freezing system gradually evolving toward the structure obtained upon slow freezing. In the core, crystallization typically initiates near the surface, and within approximately 20 ns, multiple crystallites form independently.

The surface crystallites define a triangular prism-like droplet shape, which is more regular upon slow cooling and more irregular upon fast cooling, due to insufficient time for relaxation. Crystallization is predominantly surface-induced, with nucleation occurring either at surface planes or at their edges. The angles between bulk crystallites and the adjacent surface planes are typically greater than 70°, indicating that the surface acts as a nucleation center rather than a structural template.

Both surface and core crystallization proceed via heterogeneous nucleation, consistently initiated by surfactant molecules. All crystallites, both at the surface and in the core, remain in a rotator phase over extended simulation times (> hundreds of ns) which is in agreement with the observed droplet deformation, a phenomenon expected to occur only in the presence of a rotator phase [43]. This result highlights a fundamental difference in phase behavior: while the rotator phase in bulk hexadecane is transient and rapidly transforms into the triclinic phase, it is stabilized under confinement within droplets, in correspondence with experimental observations.

While the quantitative values reported here are specific to the investigated system and simulation conditions, the simulations provide qualitative mechanistic insights into stochastic nucleation, the influence of the cooling protocol on molecular ordering, and surface-induced crystallization in surfactant-stabilized droplets. Although additional simulations involving a broader range of systems are required to establish the generality of these observations, the trends identified in this work are consistent with our previous simulations [39-42] and with available experimental observations [43-45].

Acknowledgements

This study was funded by the Bulgarian Ministry of Education and Science, under the National Research Program "VIHREN", project Rota Active (No. KP-06-DV-4/16.12.2019). The work was supported by a grant from the Swiss National Supercomputing Centre (CSCS) under project ID ch13 for the computational time. S.T. acknowledges the support received from European

Union-NextGenerationEU, through the National Recovery and Resilience Plan of the Republic of Bulgaria, project No BG-RRP-2.004-0008.

Contributions

Sonya Tsibranska-Gyoreva: Investigation, Formal analysis, Data curation, Writing - Original Draft, Resources, Conceptualization; Stoyan Iliev: Investigation, Formal analysis, Software, Visualization; Slavka Tcholakova: Validation, Writing - Review & Editing, Project administration; Anela Ivanova: Methodology, Conceptualization, Resources, Supervision, Project administration, Writing - Review & Editing; Nikolai Denkov - Conceptualization, Validation, Writing - Review & Editing, Funding acquisition

Supporting Information

The following data are available as Supporting Information: Analysis procedures; Molecular structure of hexadecane with designated distance used to assign frozen molecules (Figure S1); Angles between pairs of surface planes and bulk crystallites originating from them (Table S1); P2 profiles of all crystallites in the core of the 300K-278K system (Figure S2); P2 profiles of all crystallites in the shell of 300K-278K system (Figure S3); P2 profiles of all crystallites in the core of 350K-278K system (Figure S4); P2 profiles of all crystallites in the shell of 350K-278K system (Figure S5); RDF profiles of all crystallites in the core of 300K-278K system (Figure S6); RDF profiles of all crystallites in the shell of 300K-278K system (Figure S7); RDF profiles of all crystallites in the core of 350K-278K system (Figure S8); RDF profiles of all crystallites in the shell of 350K-278K system (Figure S9).

References

1 Li, N.; Pang, Y.; Sun, Z.; Li, W.; Sun, Y.; Sun, X.; Liu, Y.; Li, B.; Wang, Z.; Zeng, H. Effects of Surfactants on Droplet Deformation and Breakup in Water-in-Oil Emulsions under DC Electric Field: A Molecular Dynamics Study. Fuel 2024, 358, 130328. https://doi.org/10.1016/j.fuel.2023.130328

2 Qi, Z.; Sun, Z.; Li, N.; Chen, Q.; Liu, W.; Li, W. Effect of inorganic salt concentration and types on electrophoretic migration of oil droplets in oil-in-water emulsion: A molecular dynamics study. J. Mol. Liq. 2022, 367, 120549. https://doi.org/10.1016/j.molliq.2022.120549

3 Li, N.; Sun, Z.; Sun, J.; Liu, W.; Wei, L.; Li, T.; Li, B.; Wang, Z. Deformation and breakup mechanism of water droplet in acidic crude oil emulsion under uniform electric field: A molecular dynamics study. Colloids Surf., A 2022, 632, 127746. https://doi.org/10.1016/j.colsurfa.2021.127746

4 Li, N.; Sun, Z.; Pang, Y.; Qi, Z.; Liu, W.; Li, W.; Sun, M.; Li, B.; Wang, Z. Microscopic mechanism for electrocoalescence of water droplets in water-in-oil emulsions containing surfactant: A molecular dynamics study. Sep. Purif. Technol. 2022, 289, 120756. https://doi.org/10.1016/j.seppur.2022.120756

5 Cheng, Y.; Yuan, S. Emulsification of Surfactant on Oil Droplets by Molecular Dynamics Simulation. Molecules 2020, 25, 3008. https://doi.org/10.3390/molecules25133008

6 Liu, S.; Zhang, H.; Yuan, S.; Yuan, S. Effects of Surfactants on Oil Droplet Demulsification in Oil-in-Water Emulsions under an Electric Field: A Molecular Dynamics Study. ACS Omega 2024, 9, 48232–48245. https://doi.org/10.1021/acsomega.4c05623

7 Liu, S.; Yuan, S.; Zhang, H. Molecular Dynamics Simulation for the Demulsification of O/W Emulsion under Pulsed Electric Field. Molecules 2022, 27, 2559. https://doi.org/10.3390/molecules27082559

8 Zhang, H.; Liu, S.; Wang, X.; Yuan, S.; Yuan, S. Molecular dynamics study on emulsified oil droplets with nonionic Surfactants. J. Mol. Liq. 2022, 346, 117102. https://doi.org/10.1016/j.molliq.2021.117102

9 Yang, J.; Koplik, J.; Banavar, J. R. Molecular dynamics of drop spreading on a solid surface. Phys. Rev. Lett. 1991, 67, 3539–3542. https://doi.org/10.1103/PhysRevLett.67.3539

10 Park, J.-Y.; Ha, M.-Y.; Choi, H.-J.; Hong, S.-D.; Yoon, H.-S. A study on the contact angles of a water droplet on smooth and rough solid surfaces. J. Mech. Sci. Technol. 2011, 25, 323–332. https://doi.org/10.1007/s12206-010-1218-2

11 Hwang, C.-C.; Jeng, Y.-R.; Hsu, Y.-L.; Chang, J.-G. Molecular Dynamics Simulation of Microscopic Droplet Spread on Rough Surfaces. J. Phys. Soc. Jpn. 2001, 70, 2626–2632. https://doi.org/10.1143/JPSJ.70.2626

12 Mahfud, R. Molecular Dynamics Computational Study of Sustainable Green Surfactant for Application in Chemical Enhanced Oil Recovery. ACS Omega 2024, 9, 27177–27191. https://doi.org/10.1021/acsomega.4c01332

13 Heine, D. R.; Grest, G. S.; Webb, E. B., III. Spreading dynamics of polymer nanodroplets in cylindrical geometries. Phys. Rev. E 2004, 70, 011606. https://doi.org/10.1103/PhysRevE.70.011606

14 Wang, S.; Zhao, W.; Zhou, L.; Du, X. A molecular dynamics simulation of the spreading and freezing of supercooled nanodroplet impacting on ice surface. J. Mol. Liq. 2025, 422, 126973. https://doi.org/10.1016/j.molliq.2025.126973

15 Tian, Y. Y.; Ma, M. Y.; Chen, Z. Y.; Cui, K.; Du, J. F.; Yu, C.; Wang, S. L.; He, X. Collision of nanoscale water droplets: A molecular dynamics study. Phys. Fluids 2025, 37, 012025. https://doi.org/10.1063/5.0249875

16 Dong, H.; Liu, Y.; Zhou, Y.; Liu, T.; Li, M.; Yang, Z. Mechanism investigation of coalescence behaviors of conducting droplets by molecular dynamics simulations. Colloids Surf., A 2019, 570, 55-62. https://doi.org/10.1016/j.colsurfa.2019.03.014

17 Sanchouli, N.; Babaei, S.; Kanduč, M.; Molaei, F.; Ostadhassan, M. Wetting Behavior of Kerogen Surfaces: Insights from Molecular Dynamics. Langmuir 2024, 40, 5715–5724. https://doi.org/10.1021/acs.langmuir.3c03367

18 Zhou, Y.; Dong, H.; Yang, Z.; Liu, Y. Break-up behavior of droplets containing chlorine salt with the same valence cation under electric field via molecular dynamics simulation. J. Dispersion Sci. Technol. 2020, 41, 2073-2081. https://doi.org/10.1080/01932691.2019.1650756
19 Werder, T.; Walther, J. H.; Jaffe, R. L.; Halicioglu, T.; Noca, F.; Koumoutsakos, P. Molecular Dynamics Simulation of Contact Angles of Water Droplets in Carbon Nanotubes. Nano Lett. 2001, 1, 697-702. https://doi.org/10.1021/nl015640u
20 Tian, Z.-A.; Liu, R.-S.; Peng, P.; Hou, Z.-Y.; Liu, H.-R.; Zheng, C.-X.; Dong, K.-J.; Yu, A.-B. Freezing structures of free silver nanodroplets: A molecular dynamics simulation study. Phys. Lett. A 2009, 373, 1667–1671. https://doi.org/10.1016/j.physleta.2009.02.041
21 Moromisato, S.; Tseng, H.-Y.; Nagayama, G. Molecular Dynamics Study of Droplet Impinging/Freezing on Cold Surface. Kyushu Univ. Inst. Repos. 2024, 10, 805-811. https://doi.org/10.5109/7323353
22 Christenson H. Confinement effects on freezing and melting. J. Phys. Condens. Matter 2001, 13, R95-R133. https://doi.org/10.1088/0953-8984/13/11/201
23 Alba-Simionesco, C.; Coasne, B.; Dosseh, G.; Dudziak, G.; Gubbins, K.; Radhakrishnan, R.; Sliwinska-Bartkowiak, M. Effects of confinement on freezing and melting. J. Phys. Condens. Matter 2006, 18, R15–R68. https://doi.org/10.1088/0953-8984/18/6/R01
24 Huber P. Soft matter in hard confinement: phase transition thermodynamics, structure, texture, diffusion and flow in nanoporous media. J. Phys. Condens. Matter 2015, 27, 103102. https://doi.org/10.1088/0953-8984/27/10/103102
25 Huber, P.; Wallacher, D.; Albers, J.; Knorr, K. Quenching of lamellar ordering in an n-alkane embedded in nanopores. Europhys. Lett. 2004, 65, 351–357. https://doi.org/10.1209/epl/i2003-10088-0
26 Huber, P.; Soprunyuk, V. P.; Knorr, K. Structural transformations of even-numbered n-alkanes confined in mesopores. Phys. Rev. E 2006, 74, 031610. https://doi.org/10.1103/PhysRevE.74.031610
27 Wang, L.; Sui, Z.; Zhai, M.; Tian, F.; Lan, X. Physical Control of Phase Behavior of Hexadecane in Nanopores. J. Phys. Chem. C 2015, 119, 18697–18706. https://doi.org/10.1021/acs.jpcc.5b03728
28 Mukherjee P. Confinement-driven rotator-I to rotator-V phase transition of alkane. Europhys. Lett. 2017, 118, 26002. https://doi.org/10.1209/0295-5075/118/26002
29 Kumar, M.; Prasad, S.; Shankar Rao, D. Confinement-Driven Weakening of the Rotator Phase Transitions in an Alkane through a Possible Tricritical Point. Langmuir 2010, 26, 18362–18368. https://doi.org/10.1021/la1037266
30 Xie, B.; Shi, H.; Jiang, S.; Zhao, Y.; Han, C.; Xu, D.; Wang, D. Crystallization Behaviors of n-Nonadecane in Confined Space: Observation of Metastable Phase Induced by Surface Freezing. J. Phys. Chem. B 2006, 110, 14279–14282. https://doi.org/10.1021/jp063201j
31 Xie, B.; Liu, G.; Jiang, S.; Zhao, Y.; Wang, D. Crystallization Behaviors of n-Octadecane in Confined Space: Crossover of Rotator Phase from Transient to Metastable Induced by Surface Freezing. J. Phys. Chem. B 2008, 112, 13310–13315. https://doi.org/10.1021/jp712160k
32 Su, Y.; Liu, G.; Xie, B.; Fu, D.; Wang, D. Crystallization Features of Normal Alkanes in Confined Geometry. Acc. Chem. Res. 2014, 47, 192–201. https://doi.org/10.1021/ar400116c
33 Fan, Y.; Zhang, X.; Wang, X.; Li, J; Zhu, Q. Super-cooling prevention of microencapsulated phase change material. Thermochim. Acta 2004, 413, 1–6. https://doi.org/10.1016/j.tca.2003.11.006
34 Kraack, H.; Sirota, E.; Deutsch, M. Measurements of homogeneous nucleation in normal-alkanes. J. Chem. Phys. 2000, 112, 6873–6885. https://doi.org/10.1063/1.481263
35 Montenegro, R.; Landfester, K. Metastable and Stable Morphologies during Crystallization of Alkanes in Miniemulsion Droplets. Langmuir 2003, 19, 5996–6003. https://doi.org/10.1021/la027019v
36 Shinohara, Y.; Kawasaki, N.; Ueno, S.; Kobayashi, I.; Nakajima, M.; Amemiya, Y. Observation of the Transient Rotator Phase of n-Hexadecane in Emulsified Droplets with Time-Resolved Two-Dimensional Small- and Wide-Angle X-Ray Scattering. Phys. Rev. Lett. 2005, 94, 097801. https://doi.org/10.1103/PhysRevLett.94.097801
37 Shinohara, Y.; Takamizawa, T.; Ueno, S.; Sato, K.; Kobayashi, I.; Nakajima, M.; Amemiya, Y. Microbeam X-ray Diffraction Analysis of Interfacial Heterogeneous Nucleation of n-Hexadecane inside Oil-in-Water Emulsion Droplets. Cryst. Growth Des. 2008, 8, 3123–3126. https://doi.org/10.1021/cg701018x

38 Ueno, S.; Hamada, Y.; Sato, K. Controlling Polymorphic Crystallization of n-Alkane Crystals in Emulsion Droplets through Interfacial Heterogeneous Nucleation. Cryst. Growth Des. 2003, 3, 935–939. https://doi.org/10.1021/cg0300230
39 Iliev, S.; Tsibranska, S.; Kichev, I.; Tcholakova, S.; Denkov, N.; Ivanova, A. Computational Procedure for Analysis of Crystallites in Polycrystalline Solids of Quasilinear Molecules. Molecules 2023, 28, 2327. https://doi.org/10.3390/molecules28052327
40 Iliev, S.; Tsibranska, S.; Ivanova, A.; Tcholakova, S.; Denkov, N. Computational assessment of hexadecane freezing by equilibrium atomistic molecular dynamics simulations. J. Colloid Interface Sci. 2023, 638, 743–757. https://doi.org/10.1016/j.jcis.2023.01.126
41 Tsibranska, S.; Iliev, S.; Ivanova, A.; Aleksandrov, N.; Tcholakova, S.; Denkov, N. Types of phases obtained by molecular dynamics simulations upon freezing of hexadecane-containing systems. Colloids Surf. A Physicochem. Eng. Asp. 2024, 697, 134466. https://doi.org/10.1016/j.colsurfa.2024.134466
42 Tsibranska, S.; Iliev, S.; Cholakova, D.; Ivanova, A.; Tcholakova, S.; Denkov, N. Computational freezing of pentadecane. Comp. Mater. Sci. 2026, 271, 114750. https://doi.org/10.1016/j.commatsci.2026.114750
43 Cholakova, D.; Denkov, N. Rotator phases in alkane systems: In bulk, surface layers and micro/nano-confinements. Adv. Colloid Interface Sci. 2019, 269, 7–42. https://doi.org/10.1016/j.cis.2019.04.001
44 Small, D.M.. The physical chemistry of lipids. 1986
45 Cholakova, D.; Denkov, N.; Tcholakova, S.; Lesov, I.; Smoukov, S. Control of drop shape transformations in cooled emulsions. Adv. Colloid Interface Sci. 2016, 235, 90–107. https://doi.org/10.1016/j.cis.2016.06.002
46 Bussi, G.; Donadio, D.; Parrinello, M. Canonical sampling through velocity rescaling. J. Chem. Phys. 2007, 126, 014101. https://doi.org/10.1063/1.2408420
47 Berendsen, H. J. C.; Postma, J. P. M.; van Gunsteren, W. F.; DiNola, A.; Haak, J. R. Molecular dynamics with coupling to an external bath. J. Chem. Phys. 1984, 81, 3684–3690. https://doi.org/10.1063/1.448118
48 Darden, T.; York, D.; Pedersen, L. Particle mesh Ewald: An N·log(N) method for Ewald sums in large systems. J. Chem. Phys. 1993, 98, 10089–10092. https://doi.org/10.1063/1.464397
49 Essmann, U.; Perera, L.; Berkowitz, M. L.; Darden, T.; Lee, H.; Pedersen, L. G. A smooth particle mesh Ewald method. J. Chem. Phys. 1995, 103, 8577–8593. https://doi.org/10.1063/1.470117
50 Toukmaji, A. Y.; Sagui, C.; Board, J. A.; Darden, T. A. Efficient particle-mesh Ewald based approach to fixed and induced dipolar interactions. J. Chem. Phys. 2000, 113, 10913–10927. https://doi.org/10.1063/1.1324708
51 Ryckaert, J.-P.; Ciccotti, G.; Berendsen, H. J. C. Numerical integration of the cartesian equations of motion of a system with constraints: molecular dynamics of n-alkanes. J. Comput. Phys. 1977, 23, 327–341. https://doi.org/10.1016/0021-9991(77)90098-5
52 Miyamoto, S.; Kollman, P. A. Settle: An analytical version of the SHAKE and RATTLE algorithm for rigid water models. J. Comput. Chem. 1992, 13, 952–962. https://doi.org/10.1002/jcc.540130805
53 Klauda, J. B.; Venable, R. M.; Freites, J. A.; O'Connor, J. W.; Tobias, D. J.; Mondragon-Ramirez, C.; Vorobyov, I.; MacKerell, A. D., Jr.; Pastor, R. W. Update of the CHARMM All-Atom Additive Force Field for Lipids: Validation on Six Lipid Types. J. Phys. Chem. B 2010, 114, 7830–7843. https://doi.org/10.1021/jp101759q
54 Jorgensen, W. L.; Chandrasekhar, J.; Madura, J. D.; Impey, R. W.; Klein, M. L. Comparison of simple potential functions for simulating liquid water. J. Chem. Phys. 1983, 79, 926–935. https://doi.org/10.1063/1.445869
55 Jorgensen, W. L.; Madura, J. D. Temperature and size dependence for Monte Carlo simulations of TIP4P water. Mol. Phys. 1985, 56, 1381–1392. https://doi.org/10.1080/00268978500103111
56 Abraham, M. J.; Murtola, T.; Schulz, R.; Pall, S.; Smith, J. C.; Hess, B.; Lindahl, E. GROMACS: High performance molecular simulations through multi-level parallelism from laptops to supercomputers. SoftwareX 2015, 1–2, 19–25. https://doi.org/10.1016/j.softx.2015.06.001
57 Humphrey, W.; Dalke, A.; Schulten, K. VMD: Visual molecular dynamics. J. Mol. Graph. 1996, 14, 33–38. https://doi.org/10.1016/0263-7855(96)00018-5
58 The PyMOL Molecular Graphics System, Version 3.0 Schrödinger, LLC.

59 Sirota, E.; Wu, X.; Ocko, B.; Deutsch, M. What Drives the Surface Freezing in Alkanes? Phys. Rev. Lett. 1997, 79, 531–534. https://doi.org/10.1103/PhysRevLett.79.531
60 Denkov, N.; Tcholakova, S.; Lesov, I.; Cholakova, D.; Smoukov, S. Self-shaping of oil droplets via the formation of intermediate rotator phases upon cooling. Nature 2015, 528, 392–395. https://doi.org/10.1038/nature16189
61 Cholakova, D.; Denkov, N.; Tcholakova, S.; Valkova, Z.; Smoukov, S. Multilayer Formation in Self-Shaping Emulsion Droplets. Langmuir 2019, 35, 5484–5495. https://doi.org/10.1021/acs.langmuir.8b02771
62 Evans, E.; Skalak, R. Mechanics and Thermodynamics of Biomembranes; CRC Press: Boca Raton, FL, 1980.
63 Israelachvili, J. Intermolecular and Surface Forces; Academic Press: Amsterdam, 2011.
64 Denkov, N.; Cholakova, D.; Tcholakova, S.; Smoukov, S. On the Mechanism of Drop Self-Shaping in Cooled Emulsions. Langmuir 2016, 32, 7985–7991. https://doi.org/10.1021/acs.langmuir.6b01626
65 Guttman, S.; Sapir, Z.; Schultz, M.; Butenko, A.; Ocko, B.; Deutsch, M.; Slotskin, E. How faceted liquid droplets grow tails. Proc. Natl. Acad. Sci. U.S.A. 2016, 113, 493–496. https://doi.org/10.1073/pnas.1515614113
66 Kelton, K. F.; Greer, A. L. Nucleation in Condensed Matter: Applications in Materials and Biology; Elsevier: Oxford, 2010
67 Sear, R. P. Nucleation: theory and applications to protein solutions and colloidal suspensions. J. Phys.: Condens. Matter 2007, 19, 033101. https://doi.org/10.1088/0953-8984/19/3/033101